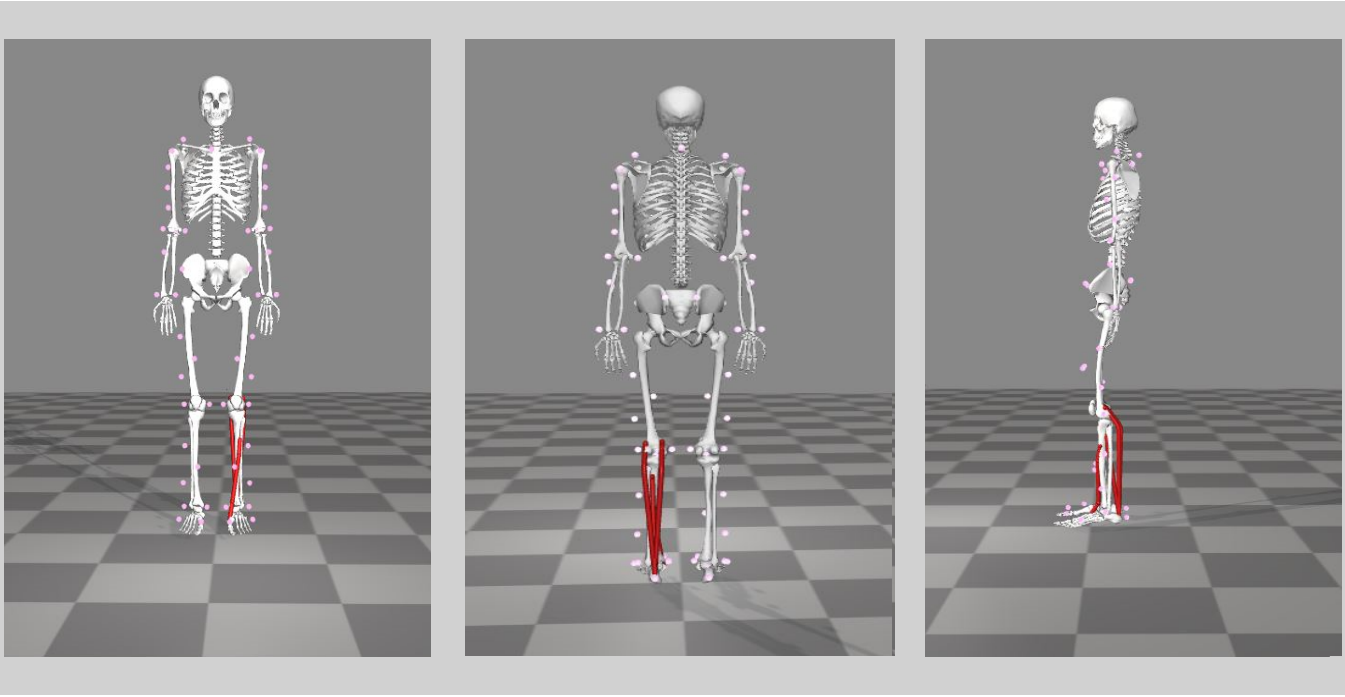

TU Delft

Calf muscle model parameters in children with cerebral palsy compared to typically developing children

Caroline Mackenbach

MSc. Thesis in Biomedical Engineering, Delft University of Technology

CALF MUSCLE MODEL PARAMETERS IN CHILDREN WITH CEREBRAL PALSY COMPARED TO TYPICALLY DEVELOPING CHILDREN

A thesis submitted to the Delft University of Technology in partial fulfillment of the requirements for the degree of

Master of Science in Biomedical Engineering

to be defended publicly on Thursday, February 11, 2021

by

Caroline Martine Mackenbach

4411455

Thesis committee:

Prof.dr.ir. J. Harlaar	Delft University of Technology
Dr.ir. A. Seth	Delft University of Technology
Dr. ing. L. Marchal Crespo	Delft University of Technology
Dr. L. Bar-On	Amsterdam UMC
Dr. M. van der Krogt	Amsterdam UMC

Amsterdam UMC
University Medical Centers

Cerebral Palsy Center of Expertise

TU Delft Delft University of Technology

ABSTRACT

Background: In children with cerebral palsy (CP), muscle-tendon structures are altered. While interventions exist to treat altered structures, the selection of the most suitable treatment is very complex with highly variable outcomes. Musculoskeletal models have the potential to support clinical decision making. However, a known limitation is the translation of altered muscle-tendon parameters into musculoskeletal models. The aim of this study was to estimate the intrinsic calf muscles properties using neuromuscular simulations of a passive ankle rotation in typically developing children and children with CP. With these simulations we determine to what extent optimal fiber length, tendon slack length, stiffness, and strain differ between typically developing (TD) and CP children.
Methods: Experimental data was collected on thirteen children with spastic CP (6 diplegia, 7 hemiplegia, age 11.6 ± 3.1 years) and 17 TD children (age 10.4 ± 3.3 years) during a slow passive ankle rotation. Ankle angle, external forces applied on the ankle, and medial gastrocnemius fascicle length were measured. An OpenSim model with four muscles around the ankle, GASM, GASL, SOL, and TA, was used to simulate passive ankle rotation experiments. Optimal fiber length, tendon slack length, stiffness at low force, strain at zero force, and strain at maximum force were optimized to match the measured ankle moment-angle curves and the GASM fascicle length-angle curves.
Results: The ankle moment-angle curves could be successfully matched in both CP (residual 0.34 ± 0.07 Nm) and TD by optimizing individual calf muscle-tendon parameters. The fascicle length-angle curves could be predicted much better in CP children by optimization, however relatively large residuals remained (residual 0.36 ± 0.13 cm). These simulations reveal that children with CP have a shorter normalized optimal fiber length and a longer triceps surae normalized tendon slack length compared to TD children. Also, CP triceps surae was found to be stiffer and undergoes less fascicle strain compared to TD children. Further, the triceps surae passive fiber force-length curve in CP children is engaged at shorter fiber lengths when compared to that of TD children.
Conclusion: Simulations show that intrinsic calf muscle-tendon properties are systematically different between CP and TD children. However, large variances in fascicle lengthening and muscle-tendon parameters in CP children exist. Future research should attempt to better match groups in terms of age, height, and weight. A next step would be to apply these optimized parameters to simulations of CP gait. This would help identify to what extent altered muscle properties affect gait in children with CP and subsequent treatment decisions.

ACKNOWLEDGEMENTS

I remember watching a TED Talk from MIT professor Hugh Herr about prosthetic limbs that inspired me to pursue a biomedical engineering degree (https://www.ted.com/talks/hugh_herr_the_new_bionics_that_let_us_run_climb_and_dance#t-1687). From that day forward, many people have guided me through the process.

Some people I would like to thank specifically. First of all, thank you dr. ir. Dick Plettenburg for motivating me and helping me with the practical aspects of the bridging program. Also, I would like to thank prof. dr. ir. Jaap Harlaar for bringing me into contact with the Motor Control Laboratory of Northwestern Medicine for my internship in the beautiful city of Chicago.
Secondly, I would like to thank my supervisors dr. ir Ajay Seth, dr. Lynn Bar-On, and dr. Marjolein van der Krogt. Thank you all for pushing me to greater heights and encouraging me to think bigger. I've enjoyed our numerous discussions which guided me through my graduation project.
I would like to thank my parents, who have supported me from day one in pursuing my dreams in becoming both a medical doctor and an engineer. Thank you, Josephine, for distracting me with our year long tradition of watching Greys Anatomy marathons. And thank you, Marc, for always being there for me and cheering me on. Thank you, Zwalua, for your carpe diem mentality and being able to celebrate every baby step in this enormous project.
Also, I would like to thank my friend ir. Rachel Oversier. You understand like no other what challenges that arise in pursuing two master's degrees. Your calming personality has helped me structure my sometimes chaotic mind and helped me find new ways to go forward.
Additionally, I would like to thank my friends who have provided me with some necessary distractions with long walks, wine nights and many laughs.

CONTENTS

1 INTRODUCTION 1
1.1 Research questions . . . 3
2 METHODS 4
2.1 Measuring ankle torque and medial gastrocnemius fascicle length . . 4
2.2 Generating subject-specific musculoskeletal models . . . 6
2.2.1 Muscle model . . . 7
2.2.2 Extracting simulated ankle torque and medial gastrocnemius fascicle length . . . 8
2.3 Fitting muscle model parameters to match the experimental data . . . 9
2.4 Statistics . . . 11
3 RESULTS 12
3.1 Subject characteristics . . . 12
3.2 Fitting of muscle parameters . . . 12
4 DISCUSSION 18
5 CONCLUSION 20
A INDIVIDUAL TORQUE–ANGLE AND NORMALIZED FASCICLE–ANGLE RESULTS 24
B INDIVIDUAL OPTIMIZED MUSCLE–TENDON PARAMETERS 29
C MEASURED AND MODELLED MOMENT–ARMS 31

LIST OF FIGURES

Figure 1.1 Framework virtual interventions 2
Figure 2.1 Overview of methodology 4
Figure 2.2 Experiment and model set-up 5
Figure 2.3 Free body diagram of the foot and footplate 5
Figure 2.4 Schematic overview of lower leg 6
Figure 2.7 Ankle moment-angle curves and fascicle length-angle curves with default OpenSim parameters 9
Figure 3.1 Ankle moment-angle curves and fascicle length-angle curves after optimization 13
Figure 3.2 Boxplot of L_{opt} and T_{sl} 15
Figure 3.3 Boxplot of K_{low}, e_{zero}, and e_{max} 16
Figure 3.4 Passive fiber-force length curve for generic and optimized muscle 17
Figure A.1 Individual TD torque-angle results 25
Figure A.2 Individual TD normalized fascicle-angle results 26
Figure A.3 Individual CP torque-angle results 27
Figure A.4 Individual CP normalized fascicle-angle results 28
Figure C.1 Measured and modelled moment-arms in TD and CP children 31

LIST OF TABLES

Table 2.1 Subject characteristics 5
Table 2.2 Design variables 9
Table 2.3 Default parameters for the fiber force-length curve 10
Table 2.4 Bound constraints for lsqcurvefit solver 10
Table 2.5 Options for lsqcurvefit solver 11
Table 3.1 ROM in CP and TD children 12
Table 3.2 Optimization results *Lopt* and *Tsl* 13
Table 3.3 Optimization results passive parameters 14
Table A.1 RMSE of the ankle moment-angle curves and the fascicle length-angle curves for each individual. 24
Table B.1 Individual optimization results *Lopt* and *Tsl* 29
Table B.2 Individual optimization results passive parameters 30

ACRONYMS

CP cerebral palsy iii
TD typically developing iii
ROM range of motion 1
MTU muscle-tendon unit 1
GMFCS Gross Motor Function Classification System 5
TA tibialis anterior 4
SOL soleus 4
GASM medial gastrocnemius 4
GASL lateral gastrocnemius 4

1 INTRODUCTION

Cerebral palsy describes a group of permanent motor disorders that are attributed to lesions in the infant brain [Rosenbaum et al., 2007]. During childhood, CP is the most prevalent motor disability, with a prevalence of 1.5 to 2.5 per 1000 live births [Graham et al., 2016]. CP is a heterogeneous condition in terms of aetiology, pathophysiology, as well as in types and severity of impairments. The most common type of CP is spastic CP [Rosenbaum et al., 2007]. Children with CP often develop gait pathology which has an enormous impact on their social and community participation [Graham et al., 2016]. In particular, the limited ankle joint movement in these children is closely related to gait and balance performance [Ballaz et al., 2010]. The limited range of motion (ROM) of the ankle is associated with adaptations in the triceps surae muscle-tendon complex.

Many interventions exist that attempt to treat these alterations, such as orthopedic surgery, often in combination with physical therapy [Graham et al., 2016]. The selection of a suitable treatment is very complex and is mainly based on clinical assessment of the patient, integrated 3D analysis and medical imaging [Molenaers et al., 2001]. The outcome of operative treatments is not always as desired. One study reported a deterioration of 22.8% of gait related parameters after orthopaedic surgery that was carried out to improve gait performance in children with CP [De Morais Filho et al., 2008].

Therefore, it is extremely important that our model reflects the adaptations and limitations of the patient if we are to understand which treatments will be most effective. In order for models to exhibit the same passive muscle stiffness properties, these parameters must be identified and tuned to the individual patient. The identification of these parameters allows for making pre-operative predictions that could guide the decision-making process towards the most effective treatments in terms of functional outcomes [Pitto et al., 2019]. Methods that rely on musculoskeletal models and computational simulations could be capable of identifying causal relations between impairments and treatment outcome [Morrison et al., 2018]. However, in order to introduce simulation-based decision-supporting tools into clinical practise, a few obstacles have yet to be overcome. First of all, the neuromusculoskeletal impairments in children with CP, such as an altered musculoskeletal geometry, altered neural control, and altered musculoskeletal parameters, must be translated into musculoskeletal models [Pitto et al., 2019]. In Figure 1.1 a framework for the development of a simulation-based decision-supporting tool are shown.

In order for models to exhibit the same passive muscle stiffness properties, these parameters must be identified and tuned to the individual patient.

Several studies have demonstrated the need of subject-specific musculoskeletal models to account for the altered musculoskeletal geometry in children with CP [Bosmans et al., 2016; Scheys et al., 2011a,b]. Also, the altered motor control, as is reflected in muscle synergies, have been used in the control of musculoskeletal models during dynamic simulations in children with CP [Kim et al., 2018; Steele et al., 2015]. Further, altered muscle-tendon properties in children with CP invalidate the use of scaled generic parameters [Falisse et al., 2016]. In this study, the focus will be on the altered passive muscle-tendon properties of the calf muscles in children with CP.

We know from literature that the medial gastrocnemius muscle-tendon unit (MTU) in children with CP is structurally different from that of TD children [Barrett and Lichtwark, 2010]. The Achilles tendon is longer and the fascicles and muscle belly

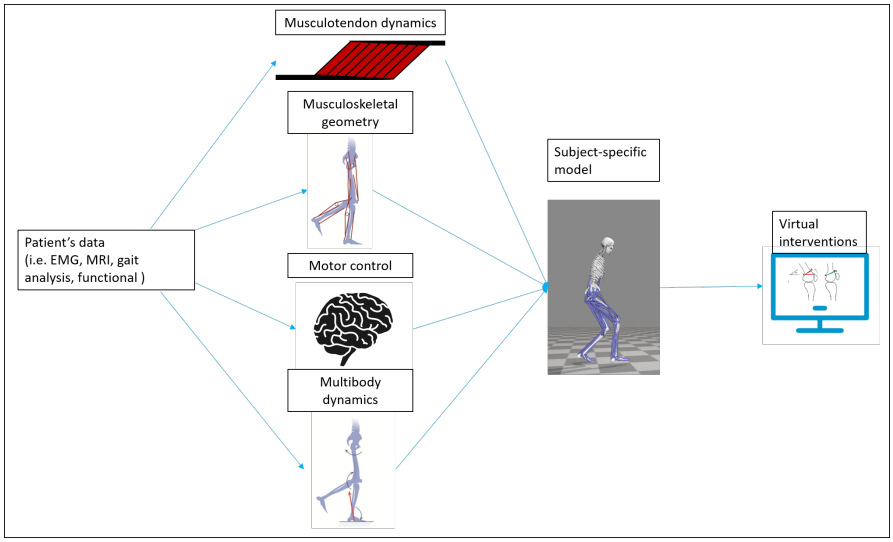

Figure 1.1: A framework for the development of a tool to evaluate the effects of virtual interventions. Data collected on the patient is used as input to generate a subject-specific model by personalizing the musculotendon dynamics and musculoskeletal geometry and by modelling the motor control and multibody dynamics. Adapted from Pitto et al. [2019] and Seth et al. [2018].

are shorter [Theis et al., 2016; Wren et al., 2010; Kalkman et al., 2018]. Also, children with CP have a higher ankle and passive muscle stiffness, which could contribute to the differences in lengthening behavior of the muscle and tendon. It might be that the increased fiber stiffness causes a greater resistance to motion at the ankle during dorsiflexion, such as in the late stance phase of walking [Alhusaini et al., 2010]. Also, the medial gastrocnemius fascicles in children with CP undergo less fascicle strain in response to a passive stretch than in TD children [Barber et al., 2011].

These altered musculoskeletal parameters make the generic Hill-type muscle model less predictive for musculoskeletal simulations in children with CP, since parameters are generally based on cadaver studies of healthy adults [Delp et al., 1990]. Thus, the generic muscle-tendon properties in the Hill-type muscle model may not capture the altered properties in children with CP, which can result in unrepresentative simulations of the muscle-tendon unit. Therefore, muscle-tendon parameters in CP musculoskeletal models should be personalized. To date, few methods have been proposed for tuning and scaling of musculoskeletal parameters. Modenese et al. [2016] developed a method that seeks to preserve the fiber operating length over the ROM that is the same as the generic model. However, this method does not address the CP related adaptations. Van Campen et al. [2014] and Falisse et al. [2016] developed a method for the estimation of muscle-tendon parameters of the knee muscles. Falisse and colleagues have investigated the effects of using personalized rather than generic muscle-tendon parameters. They modelled altered muscle-tendon properties by personalizing Hill-type muscle models based on data collected of one child with CP during functional movements. They found that the personalized optimal fiber lengths were shorter and tendon slack lengths were longer than their generic counterparts [Falisse et al., 2019]. In this study, the model relied on the experimental data collection of one child and the authors limited their parameter estimation to optimal fiber lengths and tendon slack lengths. The authors suggest that other parameters may need to be personalized to accurately capture the effect of the child's altered muscle-tendon properties.

1.1 RESEARCH QUESTIONS

The purpose of this study is to evaluate muscle-tendon parameters for a patient-specific musculoskeletal model that will help prevent post-surgery complications and help clinicians improve their pre-surgery decision making when treating children with cerebral palsy. Therefore, this study will estimate, using neuromuscular simulations, the intrinsic muscle model parameters of the calf muscles during a passive ankle rotation in children with CP and TD children. This leads to the following research questions:

- *Is there a systematic difference in optimal fiber length and tendon slack length of the triceps surae and tibialis anterior in CP and TD children?*
- *Is there a systematic difference in parameters of the passive fiber force length curve of the triceps surae and tibialis anterior in CP and TD children?*

2 METHODS

The aim of this study was to estimate the intrinsic muscle model properties of the calf muscles in CP and TD children. This was done through neuromuscular simulations of a passive ankle rotation in CP and TD children with an OpenSim model with four muscles around the ankle: the lateral gastrocnemius (GASL), medial gastrocnemius (GASM), soleus (SOL), and tibialis anterior (TA) (Fig. 2.1). First, experimental data was collected and the measured ankle moment and GASM fascicle lengths were extracted. Second, subject-specific musculoskeletal models were generated based on the individual's geometry. Further, a muscle analysis was carried out to obtain the simulated moments and GASM fascicle lengths. Finally, the muscle model parameters were optimized to match the measured ankle moment-angle curves and the GASM fascicle length-angle curves.

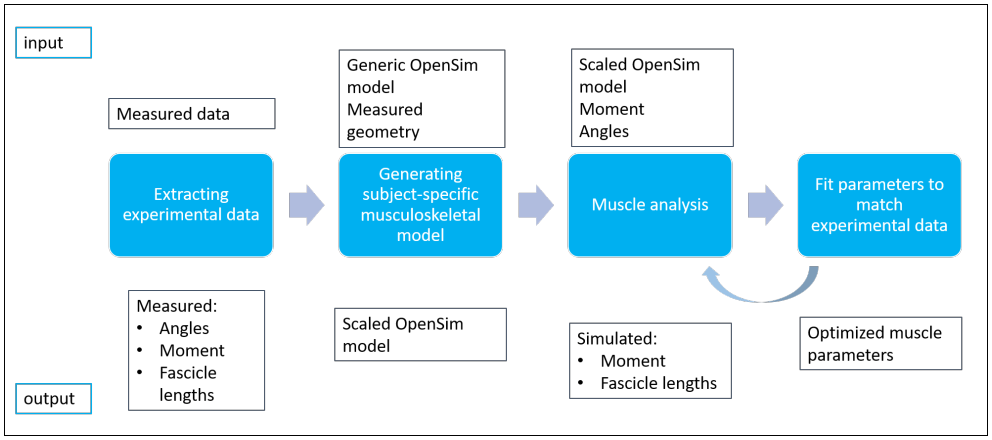

Figure 2.1: Overview of the methodology. The input and output data of each step are shown.

2.1 MEASURING ANKLE TORQUE AND MEDIAL GASTROCNEMIUS FASCICLE LENGTH

Thirteen children with spastic CP (GMFCS I or II) and 17 TD children were included in this study, with their characteristics provided in Table 2.1. All data were collected as part of a larger study [Kalkman et al., 2018]. The data collection protocol was approved by the National Health Service research ethics committee in the UK and the University Hospital's ethics committee in Leuven, Belgium. Children with CP were excluded if they had botulinum neurotoxin-A injections to the lower limb muscles 6 months before testing, a baclofen pump, any lower limb neuro- or orthopaedic surgery, or less than 20 degree of ankle movement in the sagittal plane. This was to ensure sufficient stretch in the medial gastrocnemius muscle. All TD children were free from neuromuscular or skeletal disorders.

Participants lay on a bed in prone position, with their lower leg supported at a flexion angle of 20 degrees (Fig. 2.2a). The lower leg was positioned in a orthosis to control ankle movement in the sagittal plane. The foot was manually rotated from

Group	N	Male/Female (n)	Age (years)	Height (cm)	Mass (kg)	Diplegia/Hemiplegia (n)	GMFCS (n)
CP	13	10/3	11.6 ± 3.1	143 ± 21.4	37.5 ± 19	6/7	8 I, 5 II
TD	17	8/9	10.4 ± 3.3	138.7 ± 18.6	35.5 ± 14.5	n.a.	n.a.

Values are mean ± SD, Gross Motor Function Classification System (GMFCS) [Palisano et al., 2008], n.a. not applicable.

Table 2.1: Subject characteristics

maximal plantarflexion to maximal dorsiflexion, with a maximal angular velocity of 15 ± 5 deg/s. This velocity is slow enough to not evoke a stretch reflex.

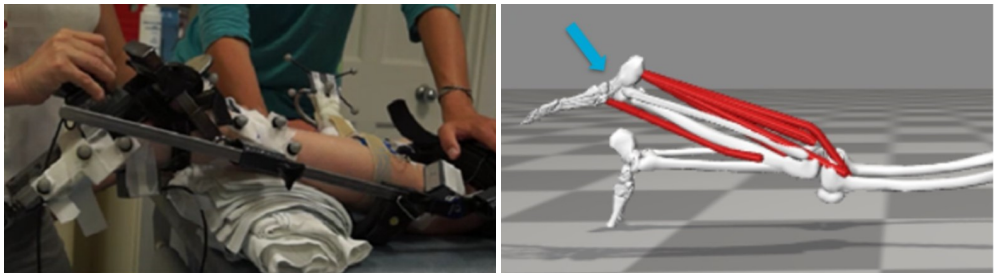

(a) (b)

Figure 2.2: Experiment and model set-up. (a) Experimental set-up, showing leg placement in orthosis. A hand-held force sensor load-cell measures net joint torque at the footplate during passive stretch. The ultrasound probe was placed on the muscle belly. Adapted from Kalkman et al. [2018]; (b) OpenSim model that is used with 4 muscles around the ankle joint and the applied force as measured experimentally as blue arrow.

Forces and torques around the ankle were measured at 200 Hz using a six degrees-of-freedom force sensor load cell, which was attached to the orthosis under the ball of the foot. Surface electromyography of the GASL and SOL was collected to evaluate neural activity. Joint trials were discarded when the RMS-EMG signal exceeded 10% of the maximal voluntary contraction value. A B-mode ultrasound scanner was secured over the MG muscle belly to measure fascicle lengthening at 30 Hz.

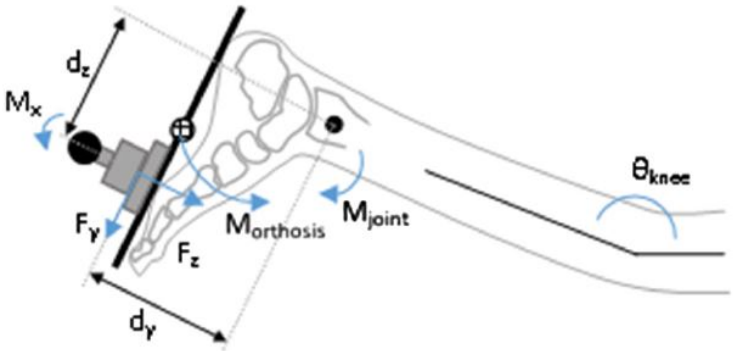

Figure 2.3: Free body diagram of the foot and footplate. The x-axis is oriented through the middle of the handle, the y-axis is oriented along the footplate. The sum of moments is given by: $M_i = F_z d_z + F_y d_y + M_x + M_{orthosis} - M_{joint}$, where dy and dz correspond to the moment arm distances from the point of force application, respectively Fy and Fz, of the load-cell to the lateral malleolus. M_x is the moment exerted on the handle about the x direction. $M_{orthosis}$ is the calculated moment caused only by the weight of the orthosis. The moment of inertia for both foot and footplate are neglected, because the mass of both is relatively small and the radius of gyration is small. Adapted from Kalkman et al. [2017].

Ankle angles were obtained from anatomical calibration of the shank and foot reference frames. Fascicle length was defined as the straight-line distance between the upper and lower aponeurosis along the lines of collagenous tissue. Fascicle lengths were calculated by semi-automatic software tracking. The net ankle joint moment was calculated from the exerted torques and forces on the load-cell and the predicted torque caused by gravity on the foot and orthotic (Fig. 2.3) [Bar-On et al., 2013]. The net ankle joint torque was then filtered with a second order Butterworth filter with a cutoff frequency of 6 Hz.

2.2 GENERATING SUBJECT-SPECIFIC MUSCULOSKELETAL MODELS

A musculoskeletal model was developed using OpenSim software [Delp et al., 2007]. The model was adapted from a generic full body musculoskeletal model that is representative of the lower-limb musculature of healthy young individuals [Rajagopal et al., 2016]. All joints were locked in 0°, except for the left knee, which was locked at 20° of flexion as imposed during the measurements, and the left ankle, which was free to move. All muscles were removed except for those around the left ankle joint: GASL, GASM, SOL, and TA muscle (Fig. 2.4).

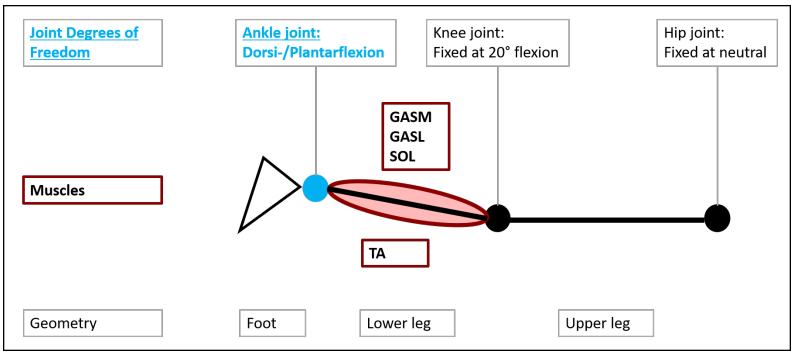

Figure 2.4: Schematic representation of the lower leg with the muscles of interest: medial gastrocnemius (GASM), lateral gastrocnemius (GASL), soleus (SOL), and tibialis anterior (TA). The model has one degree of freedom at the ankle joint. The knee and hip joints are locked.

The default activation was set to 0.01 for all muscles. The model was linearly scaled to individual subject sizes using OpenSim's scaling tool. The scaling was based on the subject's height, leg length and tibia length, which were measured during clinical examination. So, for each participant, an subject-specific musculoskeletal model was generated.
Along with the body segment sizes, optimal fiber length, tendon slack length and pennation angle are scaled by the segment length ratios. The maximal isometric muscle forces were scaled based on body mass M:

$$F^{max}_{subject} = F^{max}_{generic}\left(\frac{M_{subject}}{M_{generic}}\right)^{(2/3)} \tag{2.1}$$

where *generic* refers to the OpenSim full body musculoskeletal model [Rajagopal et al., 2016].

2.2.1 Muscle model

Each muscle-tendon unit in the OpenSim model is modelled as a Hill-type muscle model according to Millard et al. [2013]. This model uses functions to define active and passive normalized muscle-force length curves (Fig. 2.5).

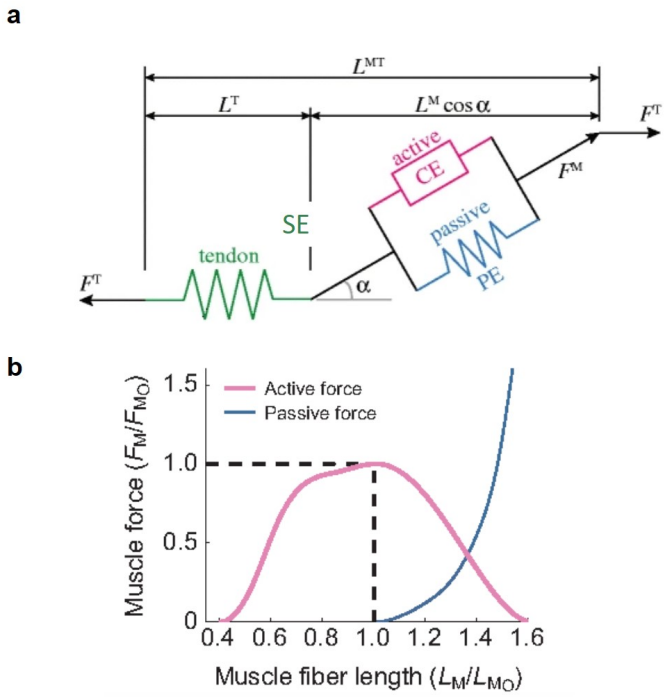

Figure 2.5: Hill-type muscle model that describes the relationship between muscle length, shortening velocity, force, and heat released during a muscle contraction. (a) The model consists of a contractile element (CE), arranged in parallel with an elastic element (PE), and a series elastic element (SE). The CE actively produces force in response to activation. The PE represents the passive forces due to the muscle's material properties in the absence of activation. The SE represents the tendon and aponeurosis. The muscle model computes muscle fiber length (L^M), muscle pennation angle (α) , tendon length (L^{MT}), muscle fiber force (F^M), and tendon force (F^T) based on the total muscle-tendon length (L^{MT}), muscle activation and the force equilibrium constraints between F^M and F^T; (b) The force-length relationship of the CE and PE. Active isometric fiber force (F_M) is normalized to maximum isometric force (F_{MO}) and fiber length (L^M) is normalized to optimal fiber length (L_{MO}). Passive fiber force was a function of normalized fiber length only. Adapted from Delp et al. [1990].

The onset of force and the slope of the fiber force-length curve of the parallel elastic component of the Millard muscle model can be adjusted by the following parameters.

- strainAtZeroForce: the fiber strain at which the fiber starts to develop force. When this parameter is zero, the fiber will begin to develop tension when it is at resting length. The definition of strain that is used in this model is: $strain = (l - l_0)/l_0$, where l is the current fiber length and l_0 is its resting length.
  It is assumed that the optimal fiber length of a muscle is also its resting length. From here on, optimal fiber length is used.
- strainAtOneNormForce: the strain at which the fiber starts to develop one unit of normalized force. When this parameter is 0.5, it means that the fiber

will develop maximum force when it is strained by 50% of its optimal fiber length.

- stiffnessAtLowForce: The normalized stiffness (i.e. slope of the force-length curve) when the fiber is just starting to develop tensile force.
- stiffnessAtOneNormForce: The normalized stiffness (i.e. slope of the force-length curve) when the fiber develops maximum force.
- curviness: a parameter that describes the shape of the force-length curve.

The parameters of the fiber force-length curve of a Millard2012 muscle in OpenSim are shown in figure 2.6.

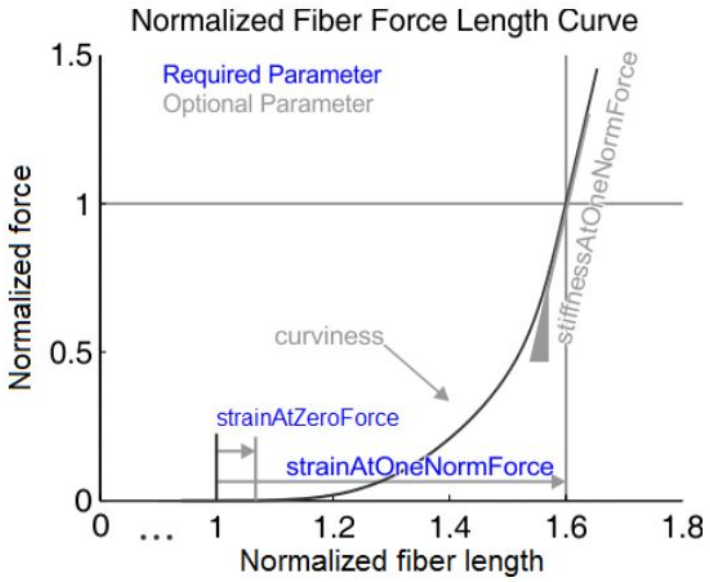

Figure 2.6: The normalized fiber force-length curve of a Millard2012 muscle in OpenSim. In blue the required properties and in grey the optional parameters. The curve is dimensionless: force is normalized to maximum isometric force and length is normalized to optimal fiber length [Millard, 2018].

2.2.2 Extracting simulated ankle torque and medial gastrocnemius fascicle length

A muscle analysis was run through the OpenSim API Analyze tool to obtain the moments and fiber lengths for each muscle individually. This was done for each participant individually using the subject-specific musculoskeletal model. The individual muscle moments were summed to obtain the net ankle moment. This was plotted against ankle angle to obtain the ankle moment-angle curve.
The GASM fascicle length was normalized to tibia length to facilitate the comparison of fascicle lengths between participants. The normalized GASM fascicle length-angle curve was plotted for each subject. Next, the individual curves were averaged to compare the fit with the averaged experimental curves.

A generic scaled muscle model does not predict the experimental ankle-moment angle curves and the GASM fascicle length-angle curves well (Fig. 2.7). The generic model overestimates the ankle moments in both CP and TD children. Also, it overestimates the normalized GASM fascicle lengthening in CP children.

Therefore, tuning of the muscle model parameters is necessary to get a better fit for the simulated torque-angle and fascicle-angle curves in both TD and CP children.

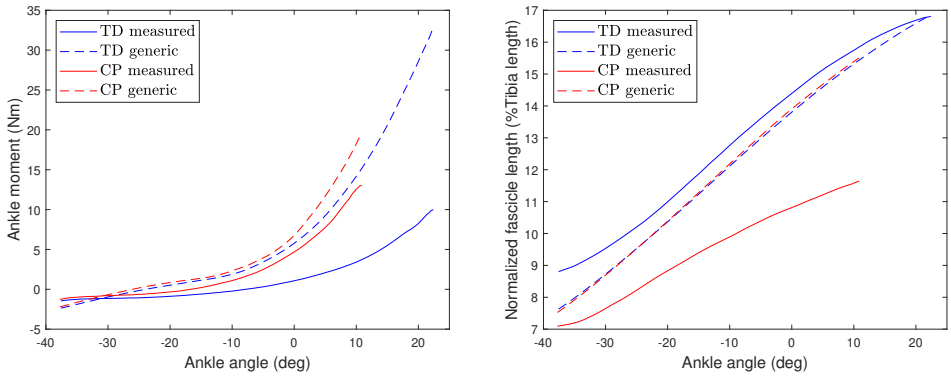

Figure 2.7: Net ankle moment-angle curves and normalized fascicle length-angle curves with generic scaled model with default muscle model parameters. Negative ankle angles indicate plantarflexion, positive values indicate dorsiflexion. (a) Net ankle moment-angle curve for typically developing (TD, blue) and cerebral palsy (CP, red) children, averaged over all subjects. Measured (solid) and simulated (dashed) results. (b) Normalized GASM fascicle length (as a percentage of tibia length) versus angle curves for typically developing (TD, blue) and cerebral palsy (CP, red) children, averaged over all subjects. Measured (solid) and simulated (dashed) results.

2.3 FITTING MUSCLE MODEL PARAMETERS TO MATCH THE EXPERIMENTAL DATA

The next step is to fit the parameters of the triceps surae and tibialis anterior muscle models to match the experimental data in a least-squares sense.
It was found that the ankle moment-angle curves and fascicle length-angle curves were most sensitive to tuning of optimal fiber length, tendon slack length, stiffness at low force, strain at zero force, and strain at maximum force. Therefore, these values were chosen as parameters for fitting. Scale factors on these parameters were introduced as design variables to reduce the number of parameters (Table 2.2).

Design variable	**Description**
$SF_{ts}L_{opt}$	scale factor on triceps surae optimal fiber length
$SF_{ta}L_{opt}$	scale factor on tibialis anterior optimal fiber length
$SF_{ts}T_{sl}$	scale factor on triceps surae tendon slack length
$SF_{ta}T_{sl}$	scale factor on tibialis anterior tendon slack length
$SF_{ts}K_{low}$	scale factor on triceps surae stiffnessAtLowForce
$SF_{ta}K_{low}$	scale factor on tibialis anterior stiffnessAtLowForce
$SF_{ts}e_{zero}$	scale factor on triceps surae strainAtZeroForce
$SF_{ta}e_{zero}$	scale factor on tibialis anterior strainAtZeroForce
$SF_{ts}e_{max}$	scale factor on triceps surae strainAtOneNormForce
$SF_{ta}e_{max}$	scale factor on tibialis anterior strainAtOneNormForce

Table 2.2: Design variables

A nonlinear least-squares solver finds coefficients for the design variables that minimizes the difference between the measured and simulated ankle moment-angle curves and GASM fascicle length-angle curves.
This problem can be written as:

$$\min_x \|F(x, xdata) - ydata\|_2^2 = \min_x \sum_i (F(x, xdata_i) - ydata_i)^2, \tag{2.2}$$

given input data $xdata$, which are the measured ankle angles and the observed output $ydata$, which is a matrix of the simulated net ankle torques and the simulated GASM fascicle lengths at each data point of $xdata$. $F(x_xdata)$ is a non-linear function that uses the scaled OpenSim muscle model to generate simulated net ankle torques and simualted GASM fiber lengths. The argument x consists of the design variables (Table 2.2).
A lsqcurvefit optimization algorithm (Matlab 2019b, The Mathworks) was used to solve equation 2.2.

Scale factors were set to a value of one as starting values, representing the default values of the the passive fiber force-length curve of a Millard2012 muscle (Table 2.3) [Millard et al., 2013]. Further, constraints were set (Table 2.4) to ensure that the optimized parameters remained within a reasonable range.

Opensim parameter	**Default value**
stiffnessAtLowForce	0.2
strainAtZeroForce	0
strainAtOneNormForce	0.7

Table 2.3: Default Opensim parameters of the fiber force-length curve of a Millard2012 muscle.

Design variable	**Lower bound**	**Upper bound**
$SF_{ts}L_{opt}$	0.5	1.5
$SF_{ta}L_{opt}$	0.5	1.5
$SF_{ts}T_{sl}$	0.5	1.5
$SF_{ta}T_{sl}$	0.5	1.5
$SF_{ts}K_{low}$	0.5	2.0
$SF_{ta}K_{low}$	0.5	2.0
$SF_{ts}e_{zero}$	-0.5	0.5
$SF_{ta}e_{zero}$	-0.5	0.5
$SF_{ts}e_{max}$	-0.5	0.5
$SF_{ta}e_{max}$	-0.5	0.5

Table 2.4: Bound constraints that were used as input arguments for the lsqcurvefit solver.

The optimization options (Table 2.5 were tuned to make sure that the optimizer converged to a solution x. Decreasing the default values for OptimalityTolerance and FunctionTolerance and increasing the default value for FiniteDifferenceStepSize led more satisfactory results. The remaining optimization options were used with default values.

For each participant, the optimal values x were saved together with the output log of the solver. For each participant, the optimized parameters were calculated by multiplying the optimal values (i.e. scale factors in x) with their respective initial values.

Option	Value
OptimalityTolerance	1×10^{-16}
FunctionTolerance	1×10^{-16}
FiniteDifferenceStepSize	1×10^{-3}

Table 2.5: The optimization options for the lsqcurvefit solver. OptimalityTolerance sets the termination tolerance on the first-order optimality, FunctionTolerance sets the termination tolerance on the function value, FiniteDifferenceStepSize sets the step size factor for finite differences.

2.4 STATISTICS

For statistical analysis, ROM, maximal dorsiflexion and plantarflexion values were compared between TD and CP children using a two-sample t-test. This test was chosen because of the normal distribution of the ROM data. The optimal parameters $Lopt$, Tsl were normalized to tibia length to control for variation in height between groups. Normalized $Lopt$ and Tsl, as well as K_{low}, e_{max}, and e_{zero} were compared between TD and CP using a Man-Whitney U test. This test was chosen because of the non-normally distributed data.

3 RESULTS

3.1 SUBJECT CHARACTERISTICS

Children with CP have a significantly smaller maximum dorsiflexion angle ($p<0.001$) and a smaller total ROM ($p<0.03$) when compared to TD children (Table 3.1).

Range (degree)	TD	CP	p-value
Max PF	-37.6 ± 8.7	-37.8 ± 7.3	p = 0.950
Max DF	22.4 ± 5.9	10.8 ± 8.5	p < 0.001
Total ROM	60.0 ± 10.1	48.6 ± 12.7	p < 0.02

Table 3.1: Range of motion in CP and TD children. Values are mean ± SD.

3.2 FITTING OF MUSCLE PARAMETERS

The measured ankle moment-angle curves could successfully be replicated by optimizing $Lopt$, Tsl, K_{low}, e_{max}, and e_{zero} (Fig. 3.1a, dashed lines). The fit for TD children was slightly better than that for children with CP, with a RMSE of 0.31 ± 0.11 Nm for TD children and 0.42 ± 0.25 Nm for children with CP.

The measured moment-angle curves in children with CP is steeper in TD children. Also, the passive forces in children with CP engage at a more plantarflexed angle than in TD children. The simulated moment-angle curves were also able to predict this behaviour.

The simulated GASM fascicle length for CP subjects improved greatly by optimization (Fig. 3.1b). The measured normalized GASM fascicle lengths in children with CP are smaller than in TD children. After optimization, this was also the case for the optimized model. However, the slope of the simulated curve was still too steep after optimization. This could not be further improved by tuning of the design variables.

The results in TD fascicle lengths were similar to the simulation with default OpenSim parameters. The fit between the fascicle length-angle curves was better for TD children than for children with CP, with a RMSE of 0.28 ± 0.17 cm for TD children and 0.40 ± 0.21 cm for CP children.

Children with CP have a significantly shorter GASL ($p = 0.01$), GASM ($p = 0.01$), SOL ($p = 0.01$), and TA ($p = 0.049$) normalized optimal fiber length when compared to TD children (Table 3.2). Also, normalized tendon slack length was significantly longer in the GASL ($p = 0.004$), GASM ($p = 0.003$), and SOL ($p = 0.01$) muscle in CP children, in comparison to TD children.
The variance between subjects in $Lopt$ and Tsl was large (Fig. 3.2 and Appendix B).

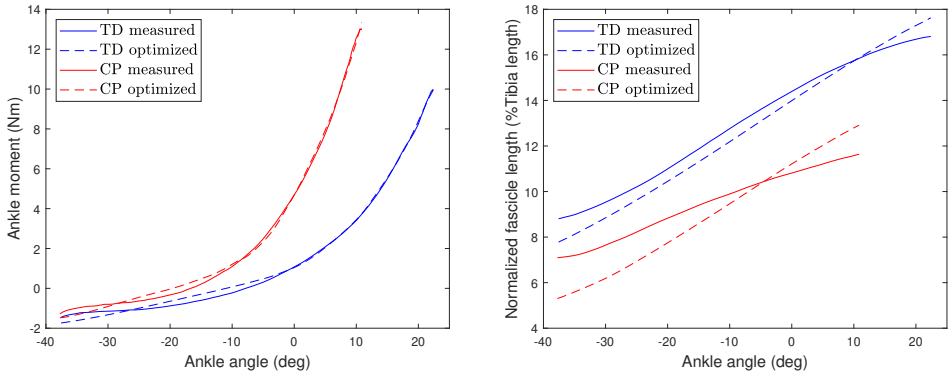

Figure 3.1: Net ankle moment-angle curves and normalized GASM fascicle length-angle curves with optimized parameters (see Table 3.2 and 3.3). Negative ankle angles indicate plantarflexion, positive values indicate dorsiflexion. (a) Net ankle moment-angle curve for typically developing (TD, blue) and cerebral palsy (CP, red) children, averaged over all subjects. Measured (solid) and optimized (dashed) results. (b) Normalized GASM fascicle length (expressed as a percentage of tibia length) versus angle curves for typically developing (TD, blue) and cerebral palsy (CP, red) children, averaged over all subjects. Measured (solid) and optimized (dashed) results.

Table 3.2: Median and interquartile range (IQR) for *Lopt* and *Tsl* after optimization for typically developing (TD) children and children with cerebral palsy (CP).

		TD				CP				
	muscle	median (norm)†	IQR (norm)†	median (cm)	IQR (cm)	median (norm)†	IQR (norm)†	median (cm)	IQR (cm)	p-value
Lopt	GASL	0.17	0.05	5.79	1.51	0.15	0.04	5.36	2.27	0.01*
	GASM	0.15	0.04	5.02	1.31	0.13	0.03	4.64	1.97	0.01*
	SOL	0.13	0.03	4.32	1.12	0.11	0.03	4.01	1.70	0.01*
	TA	0.27	0.06	8.92	2.04	0.25	0.09	8.73	2.44	0.049*
Tsl	GASL	0.95	0.25	31.46	8.18	0.98	0.02	30.90	9.03	0.004*
	GASM	1.00	0.26	33.31	8.68	1.04	0.02	32.73	9.59	0.003*
	SOL	0.70	0.18	23.09	6.00	0.72	0.01	22.60	6.56	0.01*
	TA	0.58	0.17	19.01	5.52	0.61	0.05	20.28	5.06	0.08

Lopt optimal fiber length, *Tsl* tendon slack length; † Normalized to tibia length
p-values for *Lopt* and *Tsl* were calculated after normalization; * marks significance ($p < 0.05$)

Stiffness at low force in the triceps surae was significantly higher in CP children ($p = 0.01$) compared to TD children (Table 3.3). Also, strain at zero force was smaller in CP children (0.03), even smaller than zero. This indicates that the passive fibers are engage at shorter fiber lengths when compared to both a generic muscle model and when compared to TD children. Further, strain at maximum force in the triceps surae was significantly smaller in CP children ($p = 0.003$) than in TD children. This indicates that the fibers in CP children develop more tension when they are stretched by the same force when compared to fibers in TD children. The differences between passive parameters in the tibialis anterior between CP and TD children were not significant. The variance between subjects in K_{low}, e_{zero}, e_{max} was large, especially in CP children (Fig. 3.3 and appendix B).

Table 3.3: Median and interquartile range (IQR) for K_{low}, e_{zero}, e_{max} after optimization for typically developing (TD) children and children with cerebral palsy (CP).

	muscle	default	median TD	IQR TD	median CP	IQR CP	p-value
K_{low}	triceps surae	0.2	0.14	0.04	0.20	0.05	0.01*
	tibialis anterior	0.2	0.18	0.10	0.15	0.21	0.83
e_{zero}	triceps surae	0	0.02	0.20	-0.18	0.34	0.03*
	tibialis anterior	0	-0.40	0.17	-0.32	0.45	0.28
e_{max}	triceps surae	0.7	0.73	0.14	0.59	0.21	0.003*
	tibialis anterior	0.7	1.05	0.002	1.05	0.01	0.48

K_{low} Stiffness at low force, e_{zero} strain at zero force, e_{max} strain at max force
* marks significance ($p < 0.05$)

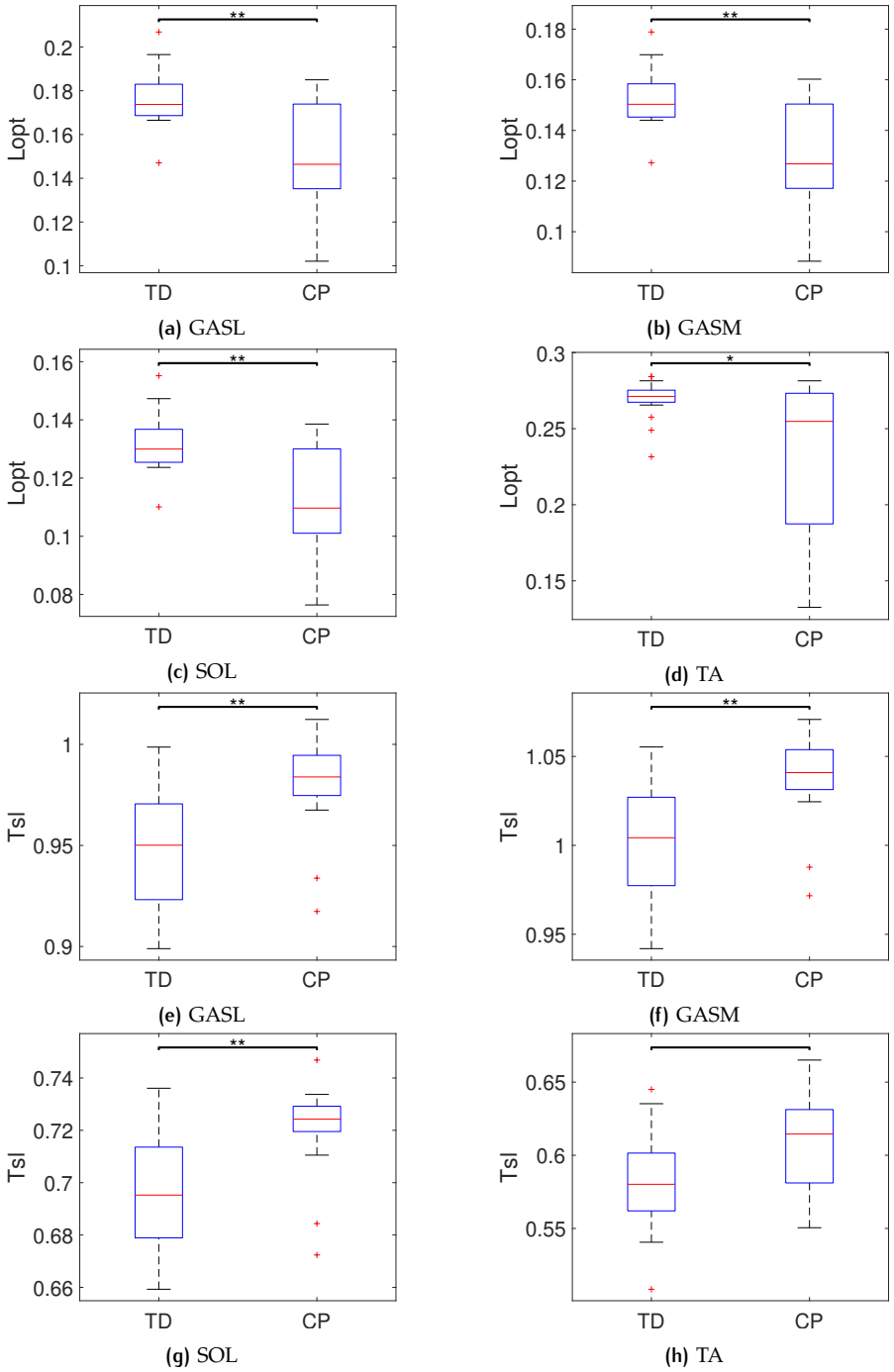

Figure 3.2: Boxplot of optimized L_{opt} and T_{sl} for typically developing (TD) and cerebral palsy (CP) for each muscle. Red line indicates median, bottom and top edges of the blue box indicate the 25th and 75th percentiles, respectively. The whiskers extend to the most extreme data points not considered outliers, and the outliers are plotted individually using the '+' symbol. Significance is marked by asteriks. * marks $p < 0.05$, ** marks $p < 1 \times 10^{-2}$. (a,e) GASL, (b,f) GASM, (c,g) SOL, (d,h) TA muscle

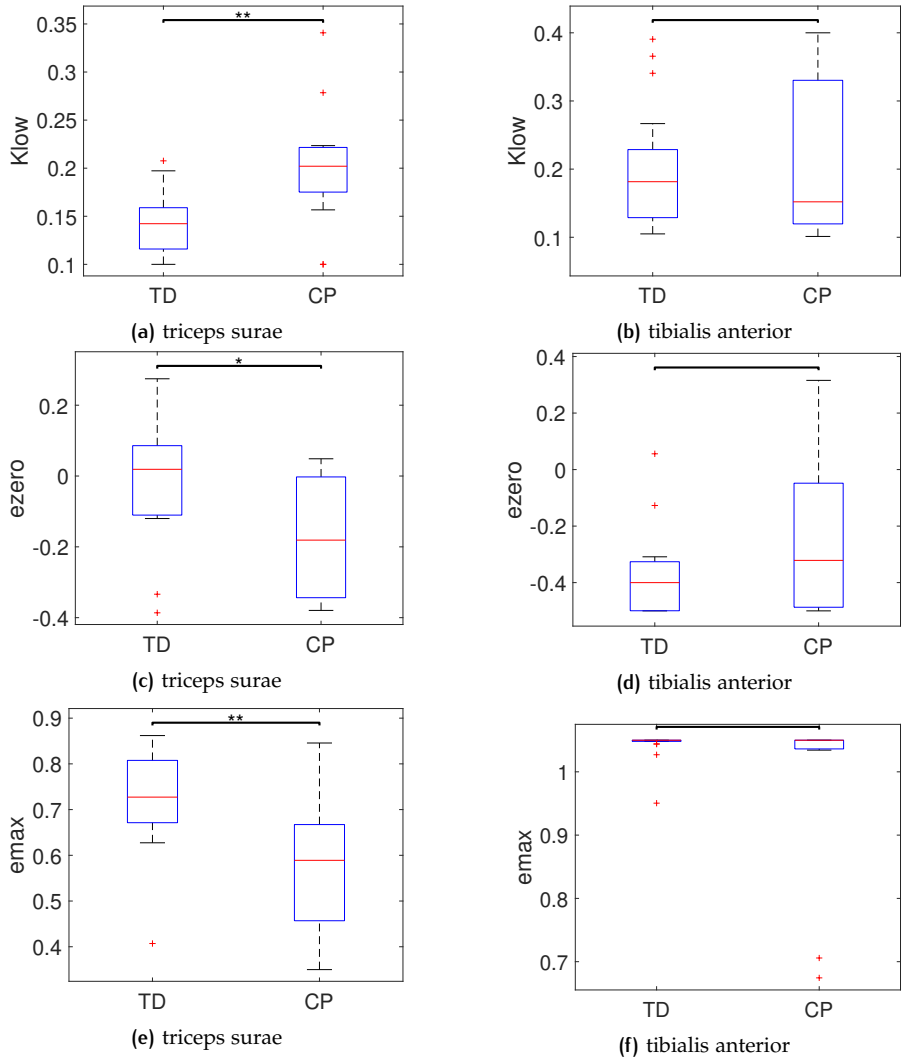

(a) triceps surae (b) tibialis anterior

(c) triceps surae (d) tibialis anterior

(e) triceps surae (f) tibialis anterior

Figure 3.3: Boxplot of optimized K_{low}, e_{zero}, and e_{max} for typically developing (TD) and cerebral palsy (CP) for each muscle. Red line indicates median, bottom and top edges of the blue box indicate the 25th and 75th percentiles, respectively. The whiskers extend to the most extreme data points not considered outliers, and the outliers are plotted individually using the '+' symbol. Significance is marked by asteriks. * marks $p < 0.05$, ** marks $p < 1 \times 10^{-2}$. (a,c,e) triceps surae, (b,d,f) tibialis anterior

The optimized GASL, GASM, and SOL passive fiber force-length curves in CP children are engaged at shorter fiber lengths when compared to that of TD children (Fig. 3.4). The generic passive fiber force-length curve in CP children is slightly different than that of TD children because of a larger generic maximum isometric forces and larger generic optimal fiber lengths. This is because the children with CP are on average taller than TD children, and thus their scaled maximum isometric forces and optimal fiber lengths are larger. The optimized GASL, GASM, and SOL passive fiber force-length curves in TD children are similar to the generic curves. This is because the optimized values for K_{low}, e_{zero}, and e_{max} are similar to the default values in the generic model.

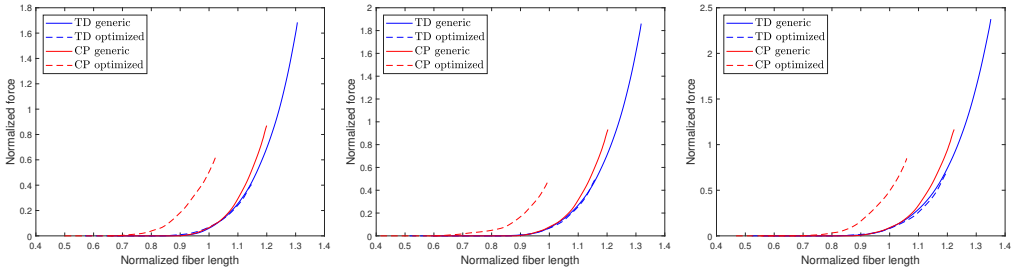

(a) GASL **(b)** GASM **(c)** SOL

Figure 3.4: Passive fiber force-length curve of the (a) GASL, (b) GASM, (c) SOL, for typically developing (TD, blue) and cerebral palsy (CP, red) children, averaged over all subjects. Generic model with default OpenSim parameters (solid) and optimized model (dashed). Force is normalized to each individual's maximum isometric force and length is normalized to each individual's optimal fiber length.

4 DISCUSSION

In this study, subject-specific musculoskeletal models were generated based on the individual's geometry and were used to estimate the intrinsic muscle model properties of the calf muscles from a passive ankle rotation in TD and CP children.

It was found that children with CP have a significantly shorter GASL, GASM, SOL, and TA normalized optimal fiber length than TD children. Further, children with CP have a significantly longer GASL, GASM, and SOL normalized tendon slack length. Falisse et al. [2019] also found a shorter optimal fiber length and a longer tendon slack length in children with CP. A longer tendon slack length in children with CP has also been confirmed in vivo [Barber et al., 2012].
In contrast, Lichtwark [2015] reported a reduction in tendon slack length of the triceps surae muscles in children with CP. The different findings on tendon slack length can be the consequence of the use of different muscle parameters in optimization. Falisse et al. [2019] optimized both optimal fiber length and tendon slack length, where Lichtwark [2015] optimized fiber slack length, fiber stiffness, and tendon slack length. Fiber slack length was defined as the relationship between optimal fiber length of the muscle and its passive slack length [Lichtwark, 2015]. Both authors attempted to simulate muscle contracture as found in experimental data, either by shortening the tendon slack length [Lichtwark, 2015], or by reducing optimal fiber length [Falisse et al., 2019] in their musculoskeletal models. The choice of different optimization parameters is based on different assumptions between these authors. Falisse et al. [2019] minimized optimal fiber length assuming that children with CP have short fibers. Lichtwark [2015] did not include optimal fiber length in his optimization parameters, because experimental data in which comparisons of fiber lengths were made between children with CP and TD children, showed inconsistent results [Barrett and Lichtwark, 2010]. Both authors based their assumptions on a systematic review about gross muscle morphology and structure in cerebral palsy [Barrett and Lichtwark, 2010]. However, more recent literature shows a consistently shorter fascicle length in children with CP throughout a common range of motion [Gao et al., 2011; Matthiasdottir et al., 2014; Kalkman et al., 2018; Barber et al., 2011]. Based on recent literature and our own findings of a longer tendon slack length in CP, we believe the findings of Falisse et al. [2019] to be more reliable.

We also found systematic differences in parameters of the passive fiber force-length curve of the triceps surae between CP and TD children. Children with CP were found to have a larger stiffness at low force, a smaller strain at zero force, and a smaller strain at maximum force. Also, the passive fiber force-length curve of the triceps surae in children with CP was altered. The passive forces engaged at a more plantarflexed angle than in TD children.
This contrasts with the findings of Lichtwark [2015], where no difference was found in fibre stiffness between CP and TD children. Again, this could be explained by the fact that this author found a shortening of tendon slack length, which also leads to an increase in fibre stiffness.
In vivo studies do confirm the findings of this study: the GASM fascicles in children with CP undergo less strain compared to controls at approximately equivalent passive ankle torques [Barber et al., 2011]. Also, Theis et al. [2016] reported a greater triceps surae muscle stiffness, although this value was calculated relative to each participants maximal force. [Alhusaini et al., 2010] also reported an increased

triceps surae stiffness, but this was only found significant between 0 and 5° dorsiflexion.
In this study, we did not find differences between CP and TD children in tibialis anterior passive muscle parameters. This could be related to the fact that the TA muscles were not fully stretched to their end range of motion in our experimental data. To better estimate the passive muscle parameters for the tibialis anterior, measurements with sufficient stretch should be included.

Optimal fiber length, tendon slack length stiffness, and strain parameters were highly variable between subjects. These variables were also substantially different from the generic muscle model parameters in children with CP. These findings affirm the importance of subject-specific musculoskeletal models with individually tuned muscle model parameters.
Further, some individual curve fits of fascicle lengthening in children with CP were better than the average fit for the group (Appendix A, Fig. A.4). Also, some individual curve fits were unsuccessfully predicted. It seems that a higher GMFCS level is related to a poor prediction of fascicle length. Most of the individual outliers have a GMFCS level II. However, a subgroup analysis is necessary to confirm this and to determine the factors that contribute to a successful prediction of fascicle length in children with CP.

A limitation of this study was the relative heterogeneity in terms of height, mass, CP diagnosis, and ROM between subjects. Consequently, it was difficult to compare the fiber force-length curve between the CP and TD children. Future studies should better match groups in terms of age, height, and weight.
Also, our subject-specific model did not account for alterations in geometry that is seen in children with CP. These alterations can also influence the musculotendon dynamics. Current literature suggests changes in Achilles moment-arm in children with CP [Kalkman et al., 2017]. Changes in Achilles tendon moment-arm would influence the moment-angle relationship and thereby the results of this study. The slope of the fascicle-angle curve in children with CP was found to be too steep, indicating an overestimation of the modelled moment-arm. However, the modelled moment-arms in the CP group are even smaller than the experimentally measured moment arms [Kalkman et al., 2017]. It should be further investigated how the moment-arms in children with CP should be modelled to get a better fit for the fascicle-angle curves.

Future studies should include richer experimental data sets. The use of experimentally collected data during isometric contractions could be helpful to find estimations of the parameters of the active fiber force-length curve. If this additional data is complemented with personalized geometry, for instance from MR images, more realistic patient-specific models could be developed [Scheys et al., 2011b].
These new optimized models could be applied to simulate gait. It would be interesting to see if an optimized model can predict the fascicle lengthening of the GASM during stance in CP children that is observed experimentally [Barber et al., 2017]. Further, this model could help identify to what extent altered muscle properties affect gait and should thus be subject to treatment.
This would be a step towards introducing clinical simulation-based decision-supporting tools into clinical practice.

5 CONCLUSION

Our simulations show that the intrinsic calf muscle-tendon properties are systematically different between CP and TD children. Children with CP have a shorter normalized optimal fiber length and a longer triceps surae normalized tendon slack length compared to TD children. Also, the triceps surae in CP children was found to be stiffer and undergoes less fascicle strain compared to TD children. The alterations in these muscle-tendon parameters can explain the torque-angle and fascicle-angle behaviour of the calf muscles during a slow passive stretch in CP and TD children. Our simulations with optimized muscle-tendon parameters can be applied to simulations of CP gait. This could help to determine to what extent alterations in muscle properties affect gait in children with CP and thereby should be subject to treatment. This would be a step forward in introducing clinical simulation-based decisions supporting tools into clinical practice.

BIBLIOGRAPHY

Alhusaini, A. A. A., Crosbie, J., Shepherd, R. B., Dean, C. M., and Scheinberg, A. (2010). Mechanical properties of the plantarflexor musculotendinous unit during passive dorsiflexion in children with cerebral palsy compared with typically developing children. *Developmental Medicine and Child Neurology*, 52(6):E101–E106.

Ballaz, L., Plamondon, S., and Lemay, M. (2010). Ankle range of motion is key to gait efficiency in adolescents with cerebral palsy. *Clinical Biomechanics*, 25(9):944–948.

Bar-On, L., Aertbeliën, E., Wambacq, H., Severijns, D., Lambrecht, K., Dan, B., Huenaerts, C., Bruyninckx, H., Janssens, L., Van Gestel, L., et al. (2013). A clinical measurement to quantify spasticity in children with cerebral palsy by integration of multidimensional signals. *Gait & posture*, 38(1):141–147.

Barber, L., Barrett, R., and Lichtwark, G. (2011). Passive muscle mechanical properties of the medial gastrocnemius in young adults with spastic cerebral palsy. *Journal of Biomechanics*, 44(13):2496–2500.

Barber, L., Barrett, R., and Lichtwark, G. (2012). Medial gastrocnemius muscle fascicle active torque-length and achilles tendon properties in young adults with spastic cerebral palsy. *Journal of Biomechanics*, 45(15):2526–2530.

Barber, L., Carty, C., Modenese, L., Walsh, J., Boyd, R., and Lichtwark, G. (2017). Medial gastrocnemius and soleus muscle-tendon unit, fascicle, and tendon interaction during walking in children with cerebral palsy. *Developmental Medicine and Child Neurology*, 59(8):843–851.

Barrett, R. S. and Lichtwark, G. A. (2010). Gross muscle morphology and structure in spastic cerebral palsy: a systematic review. *Developmental Medicine and Child Neurology*, 52(9):794–804.

Bosmans, L., Jansen, K., Wesseling, M., Molenaers, G., Scheys, L., and Jonkers, I. (2016). The role of altered proximal femoral geometry in impaired pelvis stability and hip control during cp gait: a simulation study. *Gait & posture*, 44:61–67.

De Morais Filho, M. C., Yoshida, R., da Silva Carvalho, W., Stein, H. E., and Novo, N. F. (2008). Are the recommendations from three-dimensional gait analysis associated with better postoperative outcomes in patients with cerebral palsy? *Gait & Posture*, 28(2):316–322.

Delp, S. L., Anderson, F. C., Arnold, A. S., Loan, P., Habib, A., John, C. T., Guendelman, E., and Thelen, D. G. (2007). Opensim: open-source software to create and analyze dynamic simulations of movement. *IEEE transactions on biomedical engineering*, 54(11):1940–1950.

Delp, S. L., Loan, J. P., Hoy, M. G., Zajac, F. E., Topp, E. L., and Rosen, J. M. (1990). An interactive graphics-based model of the lower extremity to study orthopaedic surgical procedures. *IEEE Transactions on Biomedical engineering*, 37(8):757–767.

Falisse, A., Pitto, L., Kainz, H., Hoang, H., Wesseling, M., Van Rossom, S., Papageorgiou, E., Bar-On, L., Hallemans, A., Desloovere, K., et al. (2019). Physics-based predictive simulations to explore the differential effects of motor control and

musculoskeletal deficits on gait dysfunction in cerebral palsy: a retrospective case study. *bioRxiv*, page 769042.

Falisse, A., Van Rossom, S., Jonkers, I., and De Groote, F. (2016). Emg-driven optimal estimation of subject-specific hill model muscle–tendon parameters of the knee joint actuators. *IEEE Transactions on Biomedical Engineering*, 64(9):2253–2262.

Gao, F., Zhao, H., Gaebler-Spira, D., and Zhang, L. Q. (2011). In vivo evaluations of morphologic changes of gastrocnemius muscle fascicles and achilles tendon in children with cerebral palsy. *American Journal of Physical Medicine Rehabilitation*, 90(5):364–371.

Graham, H., Rosenbaum, P., Paneth, N., Dan, B., Lin, J., Damiano, D., Becher, J., Gaebler-Spira, D., Colver, A., Reddihough, D., Crompton, K., and Lieber, R. (2016). Cerebral palsy. *Nature Reviews Disease Primers*, 2.

Kalkman, B. M., Bar-On, L., Cenni, F., Maganaris, C. N., Bass, A., Holmes, G., Desloovere, K., Barton, G. J., and O'Brien, T. D. (2017). Achilles tendon moment arm length is smaller in children with cerebral palsy than in typically developing children. *Journal of Biomechanics*, 56:48–54.

Kalkman, B. M., Bar-On, L., Cenni, F., Maganaris, C. N., Bass, A., Holmes, G., Desloovere, K., Barton, G. J., and O'Brien, T. D. (2018). Muscle and tendon lengthening behaviour of the medial gastrocnemius during ankle joint rotation in children with cerebral palsy. *Experimental Physiology*, 103(10):1367–1376.

Kim, Y., Bulea, T. C., and Damiano, D. L. (2018). Children with cerebral palsy have greater stride-to-stride variability of muscle synergies during gait than typically developing children: implications for motor control complexity. *Neurorehabilitation and neural repair*, 32(9):834–844.

Lichtwark, G. (2015). Simulating the effect of contracture and weakness on walking capacity in cerebral palsy.

Matthiasdottir, S., Hahn, M., Yaraskavitch, M., and Herzog, W. (2014). Muscle and fascicle excursion in children with cerebral palsy. *Clinical Biomechanics*, 29(4):458–462.

Millard, M. (2018). Opensim::fiberforcelengthcurve class reference.

Millard, M., Uchida, T., Seth, A., and Delp, S. L. (2013). Flexing computational muscle: modeling and simulation of musculotendon dynamics. *Journal of biomechanical engineering*, 135(2).

Modenese, L., Ceseracciu, E., Reggiani, M., and Lloyd, D. G. (2016). Estimation of musculotendon parameters for scaled and subject specific musculoskeletal models using an optimization technique. *Journal of biomechanics*, 49(2):141–148.

Molenaers, G., Desloovere, K., De Cat, J., Jonkers, I., De Borre, L., Pauwels, P., Nijs, J., Fabry, G., and De Cock, P. (2001). Single event multilevel botulinum toxin type a treatment and surgery: similarities and differences. *European journal of neurology*, 8:88–97.

Morrison, T. M., Pathmanathan, P., Adwan, M., and Margerrison, E. (2018). Advancing regulatory science with computational modeling for medical devices at the fda's office of science and engineering laboratories. *Frontiers in medicine*, 5:241.

Palisano, R. J., Rosenbaum, P., Bartlett, D., and Livingston, M. H. (2008). Content validity of the expanded and revised gross motor function classification system. *Developmental Medicine & Child Neurology*, 50(10):744–750.

Pitto, L., Kainz, H., Falisse, A., Wesseling, M., Van Rossom, S., Hoang, H., Papageorgiou, E., Hallemans, A., Desloovere, K., Molenaers, G., et al. (2019). Simcp: A simulation platform to predict gait performance following orthopedic intervention in children with cerebral palsy. *Frontiers in neurorobotics*, 13:54.

Rajagopal, A., Dembia, C. L., DeMers, M. S., Delp, D. D., Hicks, J. L., and Delp, S. L. (2016). Full-body musculoskeletal model for muscle-driven simulation of human gait. *IEEE transactions on biomedical engineering*, 63(10):2068–2079.

Rosenbaum, P., Paneth, N., Leviton, A., Goldstein, M., Bax, M., Damiano, D., Dan, B., Jacobsson, B., et al. (2007). A report: the definition and classification of cerebral palsy april 2006. *Dev Med Child Neurol Suppl*, 109(suppl 109):8–14.

Scheys, L., Desloovere, K., Spaepen, A., Suetens, P., and Jonkers, I. (2011a). Calculating gait kinematics using mr-based kinematic models. *Gait & posture*, 33(2):158–164.

Scheys, L., Desloovere, K., Suetens, P., and Jonkers, I. (2011b). Level of subject-specific detail in musculoskeletal models affects hip moment arm length calculation during gait in pediatric subjects with increased femoral anteversion. *Journal of biomechanics*, 44(7):1346–1353.

Seth, A., Hicks, J. L., Uchida, T. K., Habib, A., Dembia, C. L., Dunne, J. J., Ong, C. F., DeMers, M. S., Rajagopal, A., Millard, M., et al. (2018). Opensim: Simulating musculoskeletal dynamics and neuromuscular control to study human and animal movement. *PLoS computational biology*, 14(7):e1006223.

Steele, K. M., Rozumalski, A., and Schwartz, M. H. (2015). Muscle synergies and complexity of neuromuscular control during gait in cerebral palsy. *Developmental Medicine & Child Neurology*, 57(12):1176–1182.

Theis, N., Mohagheghi, A. A., and Korff, T. (2016). Mechanical and material properties of the plantarflexor muscles and achilles tendon in children with spastic cerebral palsy and typically developing children. *Journal of Biomechanics*, 49(13):3004–3008.

Van Campen, A., Pipeleers, G., De Groote, F., Jonkers, I., and De Schutter, J. (2014). A new method for estimating subject-specific muscle–tendon parameters of the knee joint actuators: a simulation study. *International journal for numerical methods in biomedical engineering*, 30(10):969–987.

Wren, T. A. L., Cheatwood, A. P., Rethlefsen, S. A., Hara, R., Perez, F. J., and Kay, R. M. (2010). Achilles tendon length and medial gastrocnemius architecture in children with cerebral palsy and equinus gait. *Journal of Pediatric Orthopaedics*, 30(5):479–484.

A INDIVIDUAL TORQUE-ANGLE AND NORMALIZED FASCICLE-ANGLE RESULTS

Table A.1: RMSE of the ankle moment-angle curves and the fascicle length-angle curves for each individual.

RMSE	Moment-angle curve (Nm)	Fascicle length-angle curve (cm)
TD01	0.26	0.18
TD02	0.37	0.25
TD03	0.14	0.24
TD04	0.47	0.70
TD05	0.24	0.39
TD06	0.42	0.16
TD07	0.17	0.39
TD08	0.38	0.37
TD09	0.33	0.47
TD10	0.16	0.11
TD11	0.37	0.39
TD12	0.28	0.44
TD13	0.35	0.09
TD14	0.14	0.12
TD15	0.41	0.27
TD16	0.47	0.17
TD17	0.22	0.10
CP01	0.47	0.17
CP02	0.28	0.41
CP03	0.17	0.36
CP04	0.75	0.26
CP05	0.85	0.60
CP06	0.12	0.39
CP07	0.10	0.21
CP08	0.25	0.69
CP09	0.47	0.14
CP10	0.25	0.19
CP11	0.60	0.38
CP12	0.38	0.80
CP13	0.68	0.59

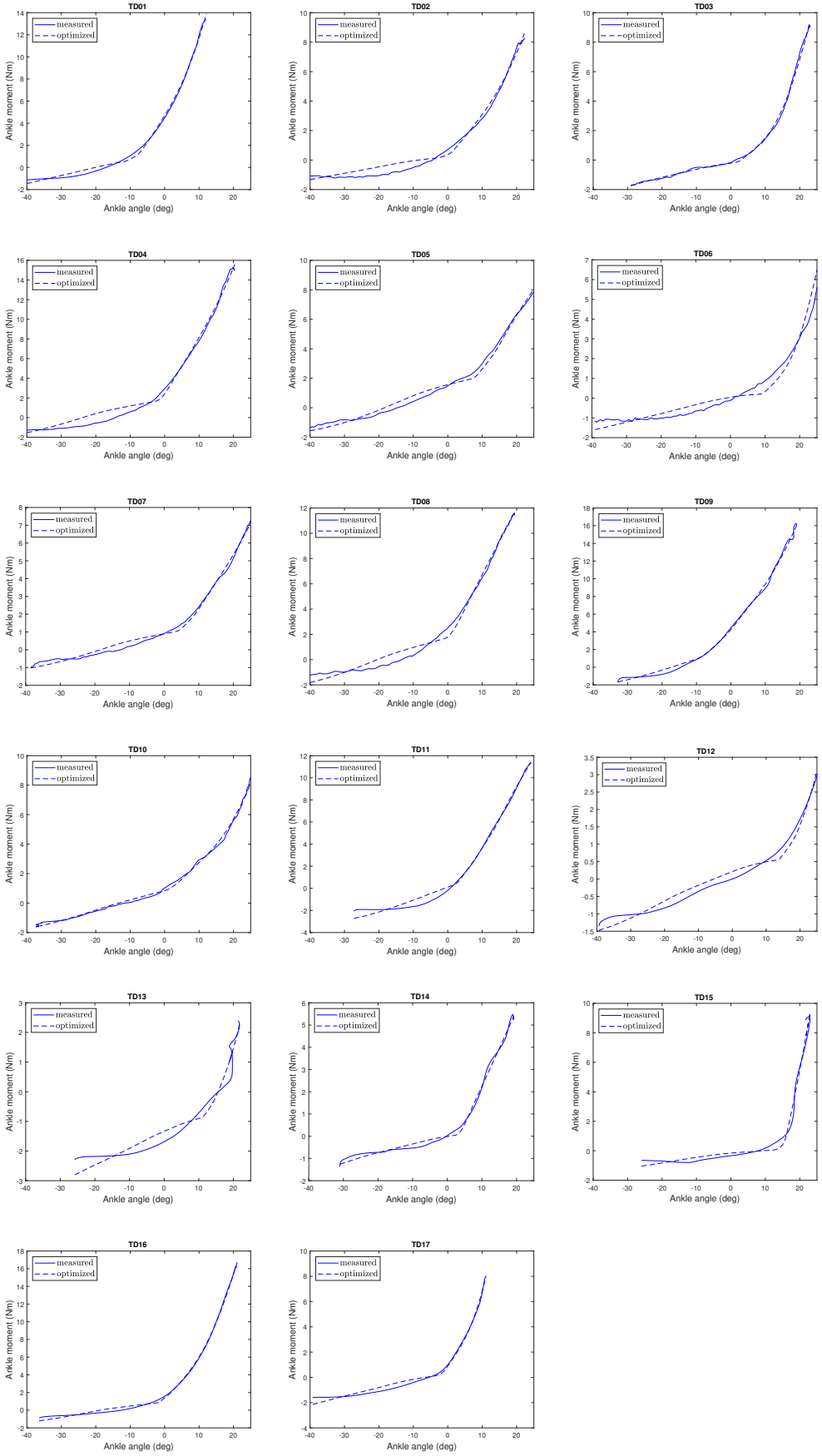

Figure A.1: Individual TD torque-angle results. Negative ankle angles indicate plantarflexion, positive values indicate dorsiflexion. Measured (solid) and simulated (dashed) results.

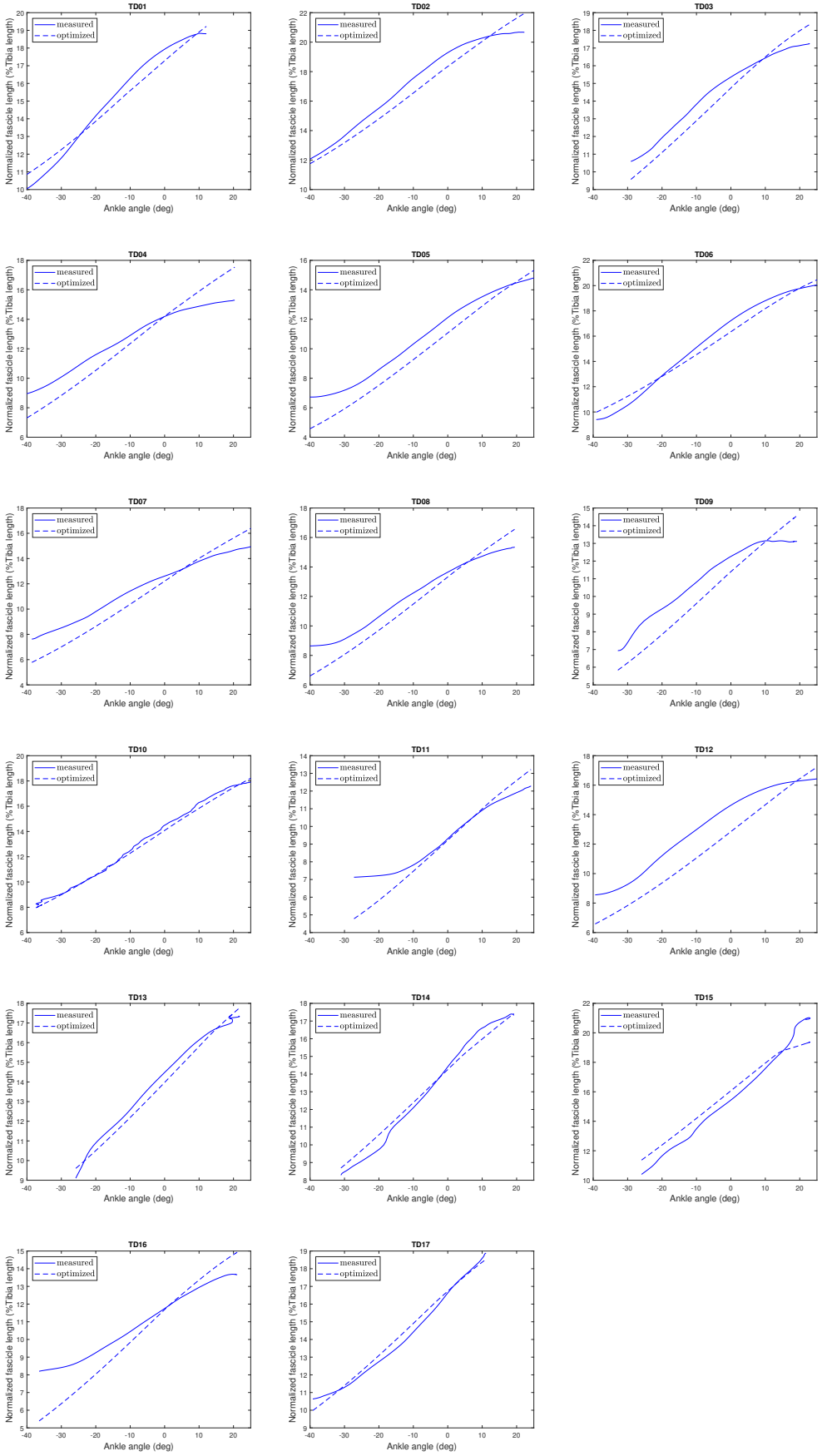

Figure A.2: Individual TD normalized GASM fascicle length (as a percentage of tibia length) versus angle curves. Negative ankle angles indicate plantarflexion, positive values indicate dorsiflexion. Measured (solid) and simulated (dashed) results.

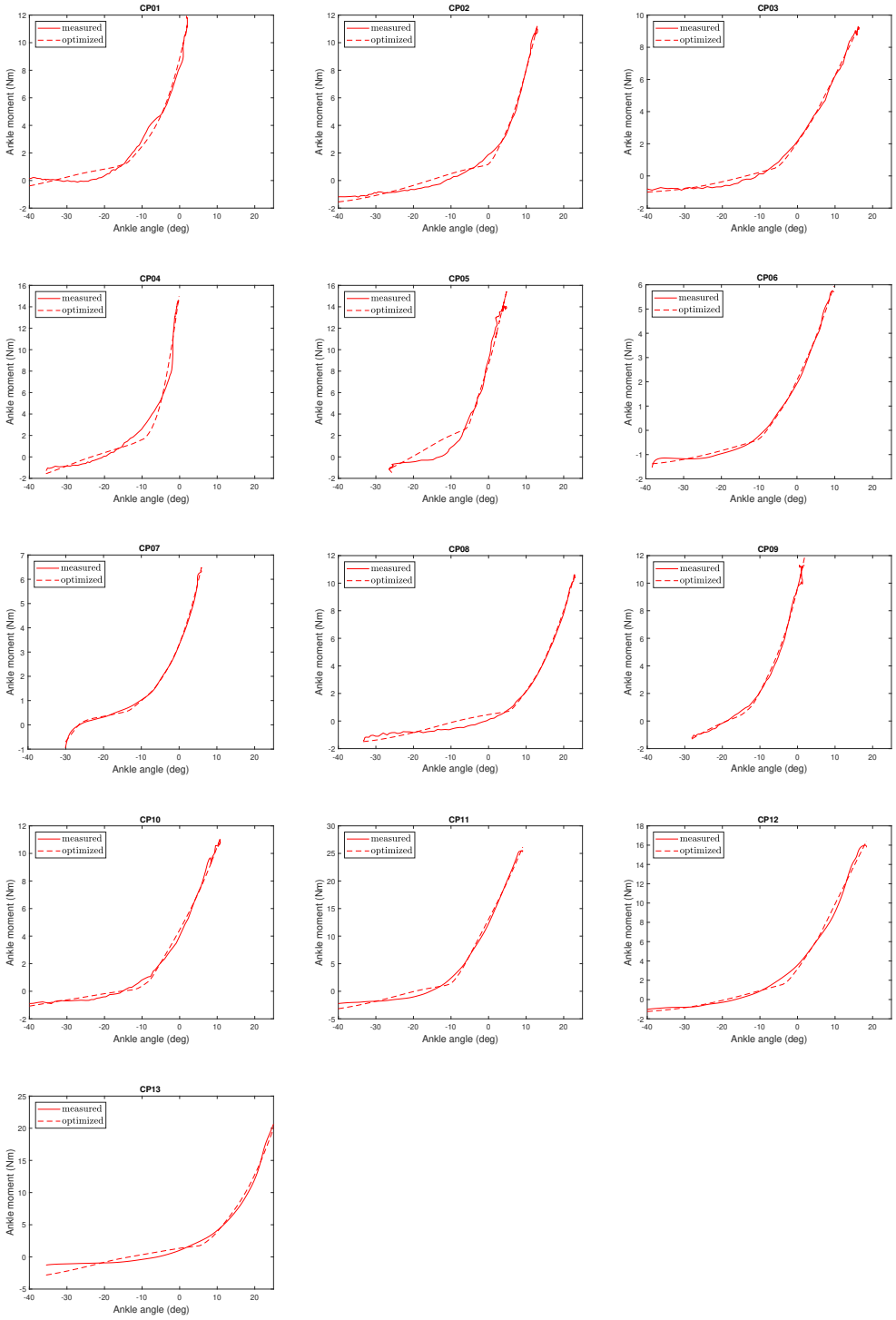

Figure A.3: Individual CP torque-angle results. Negative ankle angles indicate plantarflexion, positive values indicate dorsiflexion. Measured (solid) and simulated (dashed) results

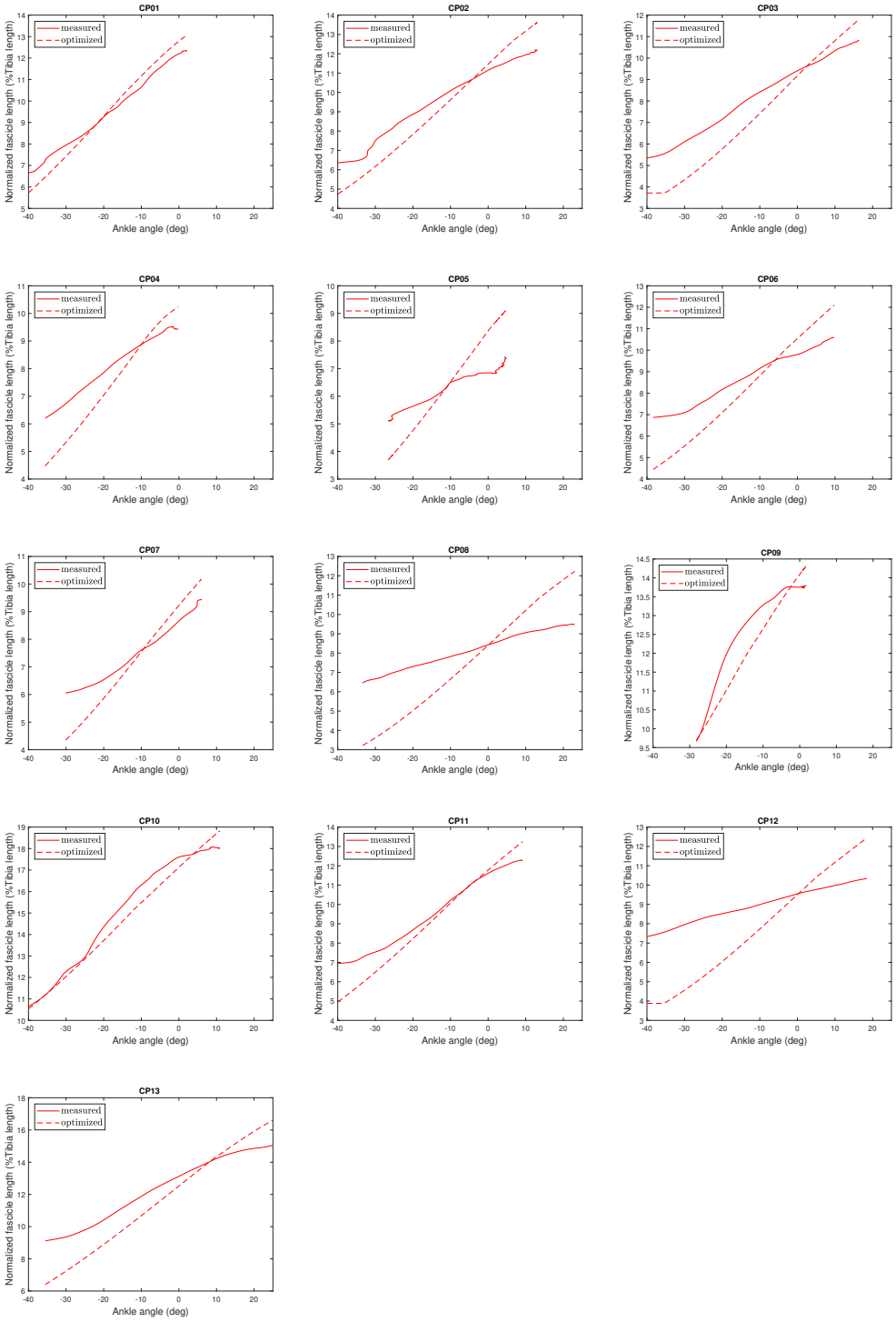

Figure A.4: Individual CP normalized GASM fascicle length (as a percentage of tibia length) versus angle curves. Negative ankle angles indicate plantarflexion, positive values indicate dorsiflexion. Measured (solid) and simulated (dashed) results.

B INDIVIDUAL OPTIMIZED MUSCLE-TENDON PARAMETERS

Table B.1: Individual results for *Lopt* and *Tsl* after optimization for typically developing (TD) children and children with cerebral palsy (CP).

	Tibia length	L_{opt} (cm)				T_{sl} (cm)			
	(cm)	GASL	GASM	SOL	TA	GASL	GASM	SOL	TA
TD01	36.0	6.05	5.24	4.50	9.56	32.73	34.67	23.93	22.87
TD02	31.0	5.83	5.05	4.35	8.73	27.87	29.47	20.44	18.21
TD03	29.0	4.94	4.27	3.70	6.71	27.26	28.80	20.08	15.68
TD04	41.0	7.43	6.43	5.56	11.05	39.13	41.42	28.78	24.44
TD05	37.0	6.43	5.56	4.81	10.07	36.24	38.34	26.67	23.39
TD06	28.0	5.05	4.37	3.75	7.96	25.68	27.18	18.79	16.78
TD07	33.0	5.86	5.07	4.38	9.01	31.98	33.84	23.50	19.01
TD08	36.5	6.42	5.56	4.80	9.97	34.95	36.99	25.68	23.54
TD09	42.0	8.69	7.51	6.52	11.26	41.25	43.60	30.43	21.36
TD10	30.0	5.70	4.93	4.24	8.43	28.27	29.92	20.70	17.23
TD11	40.0	7.86	6.80	5.89	10.85	39.95	42.21	29.44	21.76
TD12	28.0	4.73	4.09	3.52	7.96	26.61	28.16	19.47	16.07
TD13	27.0	4.50	3.89	3.34	6.72	25.27	26.75	18.46	16.42
TD14	30.5	5.08	4.39	3.81	8.24	28.98	30.63	21.36	16.56
TD15	25.0	4.25	3.61	3.23	6.44	22.67	23.55	16.95	14.68
TD16	33.0	4.85	4.20	3.63	8.92	32.19	34.05	23.70	19.15
TD17	34.0	5.79	5.02	4.32	9.30	31.46	33.31	23.09	19.31
CP01	30.0	4.03	3.49	3.03	7.47	29.31	31.01	21.70	16.77
CP02	38.0	7.03	6.09	5.27	10.11	37.48	39.69	27.61	22.24
CP03	33.0	5.68	4.91	4.25	9.10	32.75	34.60	24.09	21.36
CP04	30.5	3.11	2.69	2.33	4.04	30.01	31.75	22.09	20.28
CP05	42.0	5.12	4.43	3.84	7.78	42.52	44.97	31.37	26.03
CP06	29.5	5.36	4.64	4.01	8.04	29.02	30.69	21.36	16.76
CP07	28.0	4.10	3.55	3.05	5.27	27.83	29.49	20.38	17.43
CP08	31.0	4.20	3.64	3.12	8.73	30.90	32.73	22.60	18.35
CP09	27.5	3.76	3.25	2.80	5.07	25.68	27.16	18.82	17.95
CP10	33.0	5.43	4.71	4.05	9.10	30.27	32.07	22.19	19.97
CP11	45.0	6.59	5.70	4.94	11.96	44.12	46.71	32.51	24.77
CP12	35.0	6.27	5.43	4.68	8.80	34.97	37.04	25.68	21.51
CP13	42.0	6.76	5.85	5.05	10.70	40.63	43.03	29.84	26.29

Lopt optimal fiber length, *Tsl* tendon slack length

Table B.2: Individual results for K_{low}, e_{zero}, e_{max} after optimization for typically developing (TD) children and children with cerebral palsy (CP).

	K_{low}		e_{zero}		e_{max}	
	triceps surae	tibialis anterior	triceps surae	tibialis anterior	triceps surae	tibialis anterior
TD01	0.12	0.15	0.04	-0.50	0.86	1.05
TD02	0.14	0.16	0.09	-0.50	0.86	1.05
TD03	0.10	0.13	0.02	-0.37	0.68	1.03
TD04	0.14	0.10	-0.11	-0.50	0.70	1.05
TD05	0.16	0.15	-0.11	-0.43	0.82	1.05
TD06	0.12	0.27	0.14	-0.40	0.74	1.05
TD07	0.15	0.13	-0.11	-0.31	0.68	1.05
TD08	0.15	0.19	-0.11	-0.50	0.80	1.04
TD09	0.11	0.18	-0.39	0.06	0.41	1.05
TD10	0.10	0.37	-0.12	-0.13	0.63	1.05
TD11	0.20	0.12	-0.33	-0.32	0.78	1.05
TD12	0.16	0.20	0.09	-0.33	0.71	1.04
TD13	0.16	0.34	0.13	-0.50	0.73	0.95
TD14	0.21	0.22	0.03	-0.37	0.84	1.05
TD15	0.12	0.39	0.27	-0.33	0.65	1.05
TD16	0.14	0.11	-0.08	-0.50	0.65	1.05
TD17	0.12	0.21	0.08	-0.40	0.74	1.05
CP01	0.10	0.33	-0.12	-0.07	0.59	1.03
CP02	0.34	0.11	-0.23	-0.43	0.35	1.05
CP03	0.22	0.11	-0.36	-0.50	0.51	1.04
CP04	0.19	0.40	0.03	0.20	0.54	1.05
CP05	0.22	0.12	-0.21	-0.09	0.66	1.05
CP06	0.20	0.14	-0.38	-0.48	0.35	1.05
CP07	0.10	0.40	-0.38	0.32	0.35	0.71
CP08	0.22	0.10	-0.09	-0.50	0.60	1.05
CP09	0.22	0.34	0.00	0.03	0.65	0.67
CP10	0.20	0.20	0.05	-0.48	0.85	1.05
CP11	0.18	0.15	-0.18	-0.32	0.70	1.05
CP12	0.28	0.13	-0.34	-0.19	0.49	1.05
CP13	0.16	0.19	0.00	-0.50	0.68	1.05

K_{low} Stiffness at low force, e_{zero} strain at zero force, e_{max} strain at max force
For a full description of parameters see 2.2.1

C MEASURED AND MODELLED MOMENT-ARMS

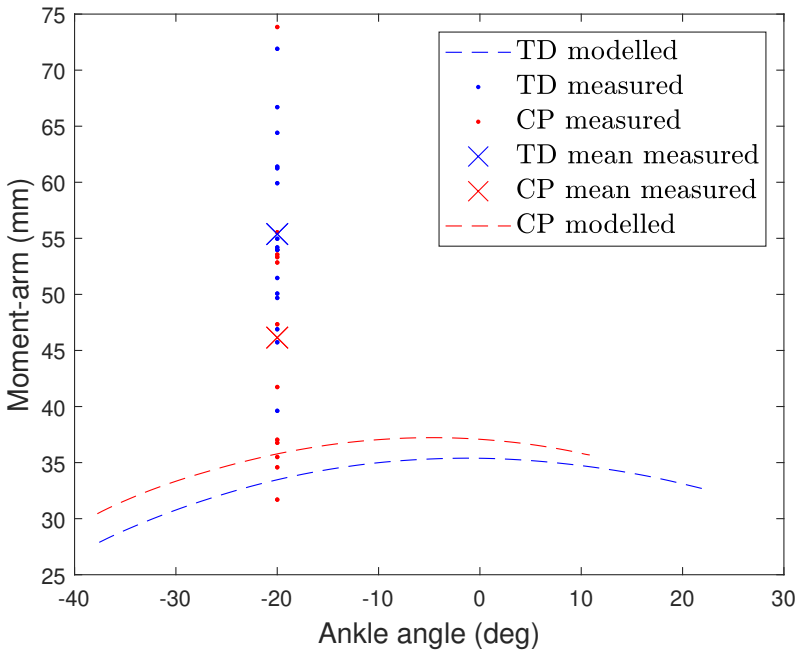

Figure C.1: Measured (dots) and modelled (dashed) GASM moment-arms in typically developing (blue) and cerebral palsy (red). Negative ankle angles indicate plantarflexion, positive values indicate dorsiflexion. Measured moment-arm data was collected as part of a larger study [Kalkman et al., 2017].